PROCEEDINGS OF SCIENCE

Final results from the MEG experiment and the status of MEG-II

Francesco Renga[*†]
INFN Rome 1
E-mail: francesco.renga@roma1.infn.it

The MEG experiment has carried on a search for the Lepton Flavour Violating decay $\mu \to e\gamma$, taking data in the 2008-2013 period. The final analysis of the MEG data is presented here, setting a new 90% confidence level upper limit on the branching ratio of this decay at 4.2×10^{-13}. We also present the status of the MEG upgrade, which is expected to improve the sensitivity by one order of magnitude within the next few years.

XIII International Conference on Heavy Quarks and Leptons
22- 27 May, 2016
Blacksburg, Virginia, USA

[*]Speaker.
[†]For the MEG Collaboration.

PoS(HQL 2016)021

1. Introduction

The standard model (SM) of particle physics is a gauge theory which, along with its structural $SU(3) \times SU(2) \times U(1)$ symmetry, comprises a non-trivial flavor structure that does not arises from this underlying gauge symmetry but follows from the specific particle content of the model, and hence can be considered to some extent *accidental*. This flavor structure includes features like the lepton flavor symmetry, which is violated by neutrino oscillation but, due to very small mass of neutrinos, is essentially conserved in the charged lepton sector. Indeed, charged lepton flavor violation (cLFV) is expected to arise from neutrino oscillations but the expected rates are largely unobservable with present technologies [1]. For instance, the cLFV decay $\mu \to e\gamma$ is expected in the SM with a branching ratio (BR) $< 10^{-50}$, while the present experimental limits are around a few 10^{-13}. On the other hand, due to the accidental nature of this symmetry, new physics (NP) models developed to overcome the theoretical limitations of the SM typically predict observable cLFV effects, unless some specific feature is introduced to suppress them. In fact, cLFV is predicted by almost any NP model and the present experimental limits already strongly constrain the development of such theories.

Supersymmetry (SUSY) is just one of the families of NP models predicting observable cLFV decays, but it is of particular interest because even if a SUSY model is built to be flavor blind at the high energy scale, cLFV terms arise in the slepton mixing matrix at the electroweak scale, through the renormalization group equations. It makes cLFV essentially unavoidable in SUSY. As a result, limits on $\mu \to e\gamma$ and similar processes give very strong constraints on SUSY models. On the other hand, one should consider that the constraints, for instance, on the mass scale of SUSY particles strongly depend on the specific flavor structure of the model. These features make the searches for NP in the cLFV sector complementary with respect to the direct searches at the LHC. Even if no NP hint is found at the LHC, there is still the possibility of observing cLFV effects from higher energy scales. Conversely, if something new is discovered at the LHC, cLFV (along with other flavor precision measurements) provides a unique way to understand the flavor structure of this NP.

Here I will report the final result of the MEG experiment, searching for the $\mu \to e\gamma$ decay at the Paul Scherrer Institut (PSI, Switzerland). I will also discuss the status of its upgrade, MEG-II, which is expected to start taking data in 2017 and improve the present limits by one order of magnitude over the next 4 years.

2. The $\mu \to e\gamma$ Signature and Backgrounds

The search for the $\mu \to e\gamma$ decay is performed by stopping muons from an intense continuous beam on a thin target, in order to exploit maximally the two-body kinematics of the decay. The positron and photon are both expected to have an energy of $m_\mu/2 \sim 52.8$ MeV, to be emitted back-to-back and at the same time. The latter information is important because, with the very high beam rates currently available (3×10^7 muons per second in MEG, more than two times more in MEG-II), the dominant background for the search of $\mu \to e\gamma$ is the accidental coincidence of a positron from a normal muon decay and a photon which can come either from a radiative muon decay (RMD) $\mu^+ \to e^+ \nu_e \overline{\nu}_\mu$ or the annihilation in flight (AIF) of another positron, which can happen e.g. in the material of the target. A sub-leading, prompt background contribution comes

from RMD themselves, where the neutrino pair is emitted with very low momentum, so that the photon and positron are almost back-to-back and with energies near the kinematical end-point.

There are hence four discriminating variables which can be used to separate signal and background: the photon energy E_γ, the positron energy E_e, the relative time $T_{e\gamma}$ and the relative angle $\Theta_{e\gamma}$. The latter is in fact replaced by two independent angles, in spherical coordinates, in order to improve its the discriminating power: $\phi_{e\gamma} = (\pi + \phi_e) - \phi_\gamma$ and $\theta_{e\gamma} = (\pi - \theta_e) - \theta_\gamma$. Both are expected to be zero for signal events.

3. The MEG Experiment

Protons from the PSI ring cyclotron are used to produce an intense muon beam (up to 10^8 muons per second can be delivered). An important feature which follows from the accidental nature of the dominant background is its dependence on the square of the muon stopping rate. It makes useless an increase of the muon rate as soon as the expected yield of background events becomes relevant ($\gg 1$). For this reason, a beam rate of 3×10^7 was found to be optimal for the MEG needs. Muons are stopped on a polyethylene/polyester target, whose thickness (205 μm) and slant angle with respect to the beam axis (70°) were optimized in terms of muon stopping rate and deterioration of the resolutions due to the interaction of the positron with the target material.

The MEG detector [2] was then designed to precisely reconstruct the discriminating variables discussed above, and is represented in Fig. 1.

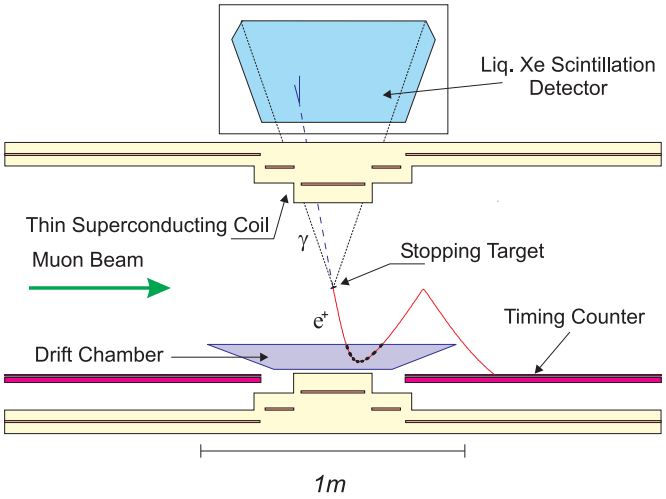

Figure 1: The MEG detector.

The photon energy was reconstructed by an 800 liter LXe electromagnetic calorimeter. The UV scintillation light emitted by the LXe was collected by 846 photomultiplier tubes (PMT). The

calorimeter was periodically calibrated using several dedicated tools. A calibration of the gain and quantum efficiency of the PMTs was performed on a weekly basis thanks to LEDs and alpha sources installed inside the detector. A weekly monitor of the energy scale was also performed exploiting a dedicated Cockroft-Walton accelerator, which was used to induce $p+Li$ and $p+B$ reactions on a Lithium tetraborate target, producing monochromatic photon lines up to 17.6 MeV. Finally, once per year, the muon beam was replaced by a pion beam to produce the charge exchange (CEX) reaction $\pi^- + p \to \pi^0 + n$ on a LHe target. The kinematics of the $\pi^0 \to \gamma\gamma$ decay produces an almost monochromatic photon line at 55 MeV, i.e. very near to the $\mu \to e\gamma$ signal peak, provided that the two photons are tagged to be almost back-to-back, thanks to a small ancillary BGO calorimeter. It allowed us to calibrate very accurately the energy scale of the detector, and provided a measurement of the energy resolution. An average resolution of about 1.9% was found.

The positron energy was reconstructed thanks to a spectrometer composed of 16 drift chambers (DC), operated with a Helium:Ethane (50:50) gas mixture in a non-uniform magnetic field. The field was maximum (1.27 T) and oriented along the beam axis at the center of the detector, where the target is placed, and then decreased along the beam axis, down to 0.49 T at the end of the magnet. This features makes tracks, even emitted at large angles with respect to the beam axis, to be expelled from the detector after no more than a few turns inside it, so to reduce the pileup in the tracking volume. Each drift chamber is composed of two planes of wires, providing a single hit resolution of about 300 μm in the radial direction. The position along the beam axis is measured thanks to patterned cathode strips with a resolution of about 1 mm. These performances, along with the very light structure of the detector ($\sim 10^{-3}$ radiation lengths over the whole track length) allowed to reach a positron energy resolution of about 300 keV. It is measured with a fit to the steep end point of the spectrum for positrons coming from the normal $\mu^+ \to e^+ \nu_e \overline{\nu}_\mu$ decay. In the final analysis of the MEG data a new feature has been introduced in the positron reconstruction: When combining multiple turns of the positron inside the spectrometer, the pattern recognition algorithm can fail to associate multiple turns to the same track, so that the propagation of the track to the target is wrong (one or more turns less than the true track). It generates an inefficiency, which has been recently reduced with the introduction of an algorithm to recover some of the missing turn. A 4% relative improvement of the efficiency has been obtained.

Concerning $T_{e\gamma}$, the LXe calorimeter provides a measurement of the photon time with 60 ps resolution. A similar resolution is guaranteed on the positron side by a dedicated detector, the timing counter (TC), which is composed of two sectors of 15 scintillating bars each. The positron reaches the TC after $\sim$ 1 meter flight from the target. Hence, the time of flight has to be subtracted to get a precise measurement of the positron emission at the target. Due to the long path of the positron from the last measurement in the DC to the TC, fluctuations of the multiple scattering and energy loss in the material between the two detectors deteriorates the resolution on the track length, which is then converted into a time of flight. The resulting contribution to the $T_{e\gamma}$ measurement is $\sim$ 100 ps. In total, a resolution of $\sim$ 130 ps is obtained on $T_{e\gamma}$. It is measured looking at the peak which can be seen in the $T_{e\gamma}$ distribution due to the prompt RMD background.

Finally, the relative angles have to be measured. Positron angles are measured by propagating the positron track from the spectrometer back to the target. It also allows us to measure the intersection of the track with the target plane, which is assumed to be the muon decay point. The photon direction is determined as the vector from the decay point to the conversion point measured

by the calorimeter with a few mm resolution. As a result, a resolution of about 15 mrad in both $\phi_{e\gamma}$ and $\theta_{e\gamma}$ is obtained. Since there is no physical process allowing for an absolute calibration of the relative angle, the resolution is extracted by combining the resolutions measured independently for the positron and the photon. In particular, the positron resolutions are determined using tracks making two turns inside the spectrometer. The two turns are treated as independent tracks and propagated to an imaginary target plane in between the two turns. The two propagated tracks are compared in order to determine the resolution on the reconstruction of the track parameters. The photon conversion point resolution is measured instead with dedicated runs where collimators are placed in front of the calorimeter. Due to the absence of a direct calibration, the measurement of the relative angle is prone to systematic uncertainties coming from a relative misalignment of all parts of the detectors. In particular, a bad alignment of the target with respect to the spectrometer can induce large systematic errors on ϕ_e, and hence $\phi_{e\gamma}$. Starting from 2012, a deformation of the target became evident. Because the target was no longer a perfect plane, a systematic uncertainty was induced on ϕ_e. Measurements using positrons and a direct 3D scan of the target have been used to get an estimate of the deformation and correct accordingly the angular measurement. Nonetheless, a non negligible systematic needed to be associated to this correction.

The geometrical acceptance of the detector was about 11%, limited by the active volume of the LXe calorimeter. A 40% photon reconstruction inefficiency was observed, mainly determined by the material in front of the LXe calorimeter (the magnet and LXe cryostat). While the positron reconstruction efficiency in the drift chamber was $\sim$ 65%, many of the these positrons could not be associated to hits in the TC because they are lost in the material between the DC and the TC. A positron efficiency of $\sim$ 30% is consequently obtained.

Another crucial component of the MEG experiment is the trigger and data acquisition (DAQ) complex. Starting from more that 10^7 muon decays per second in the detector acceptance, one needs to go down by 6 orders of magnitude with trigger in order to get a few Hz rate, manageable by the DAQ system. It is achieved thanks to a fully digital trigger implemented in FPGAs, allowing us to measure online the photon energy with a few percent resolution, the relative time with $\sim$ 1 ns resolution and to apply a rough back-to-back requirement based on the calorimeter and TC measurements. Then all the waveforms coming from the readout channels of the three sub-detectors are fully acquired for offline analysis using the DRS4 digitization chip.

4. Data Analysis and the Final Result of MEG

The four discriminating variables have been combined into a likelihood analysis to extract a limit on the BR of the $\mu \to e\gamma$ decay.

For the final analysis of the MEG data, a new feature has been introduced to reduce the probability of false positive signals. In some cases, the AIF photon producing an accidental background event comes from the interaction of a positron with the structure of a DC. In this case, a track segment can be sometimes reconstructed in the DC, ending at some point inside the spectrometer, where it points toward the conversion point reconstructed in the calorimeter. An algorithm to remove such events has been developed. It allows us to reject 1.9% of background events with a 1.1% signal inefficiency.

The likelihood analysis is then performed with a blind approach: events in a signal region defined by cuts on E_γ and $T_{e\gamma}$ are disregarded until the alignment has been fully validated on the sidebands. In particular, the sidebands allow for a very accurate estimate of the probability distribution function (PDF) for the accidental background, to be used in the likelihood analysis. Instead, the signal and RMD PDFs need to be estimated from the results of the detector calibrations. Monte Carlo simulation are only marginally used in the development of the likelihood analysis.

Two features of the likelihood analysis are worth mentioning:

1. Per-event errors are used to improve the sensitivity of the analysis. On the positron times, the per-event resolutions are extracted from the result of the track fit, performed with a Kalman Filter technique. On the photon side, the CEX calibration is performed by placing the BGO calorimeter opposite different sectors of the LXe calorimeter, allowing us to extract different photon energy resolutions depending on the photon conversion point.

2. the likelihood includes a careful treatment of correlations among the positron variables. These correlations arise from quantitatively understood geometrical reasons, related to the propagation of the track to the target plane.

After being fully tested on fake analysis regions in the sidebands, the likelihood analysis has been applied to the data collected by MEG-I from 2009 to 2013, corresponding to approximately 7.5×10^{14} muons stopped on target, resulting in a BR sensitivity around 5×10^{-13}, evaluated with toy Monte Carlo experiments. No significant signal is observed, while accidental and RMD backgrounds are in agreement with the expectations obtained from the sidebands. An upper limit of 4.2×10^{-13} is set on the BR of $\mu \to e\gamma$ at 90% confidence level, based on a frequentistic approach [3]. Data and PDFs are shown in Fig. 2. The bottom-right plot shows the event signal likelihood normalized to the background likelihood:

$$R_{\text{sig}} = \log_{10}\left(\frac{S(\mathbf{x}_i)}{f_{\text{R}}R(\mathbf{x}_i) + f_{\text{A}}A(\mathbf{x}_i)}\right) \tag{4.1}$$

where $\mathbf{x}_i$ is the set of variables in the likelihood, S, R and A the signal, RMD and accidental PDFs, and f_{R} and f_{A} the expected RMD and accidental fractions in the background (0.07 and 0.93 respectively, extrapolated from the sidebands).

5. The MEG-II Design and Status

An upgrade of the experiment [4] is currently under construction, aiming to improve the sensitivity by one order of magnitude over the next few years. Such an upgrade would be competitive with the very first phases of the searches for $\mu \to e$ conversion in the interaction with nuclei, on a shorter time scale.

The sensitive volume of the LXe calorimeter will be increased. Moreover, the PMTs in the inner face of the calorimeter will be replaced with silicon detectors (MPPC), improving the granularity and reducing the dead space between the sensors. A dedicated R&D effort has been completed in order to have MPPCs sensitive to the UV light emitted by the LXe, and the detector is currently under its final assembly phase at PSI. Along with a new geometry of the lateral faces, in order to

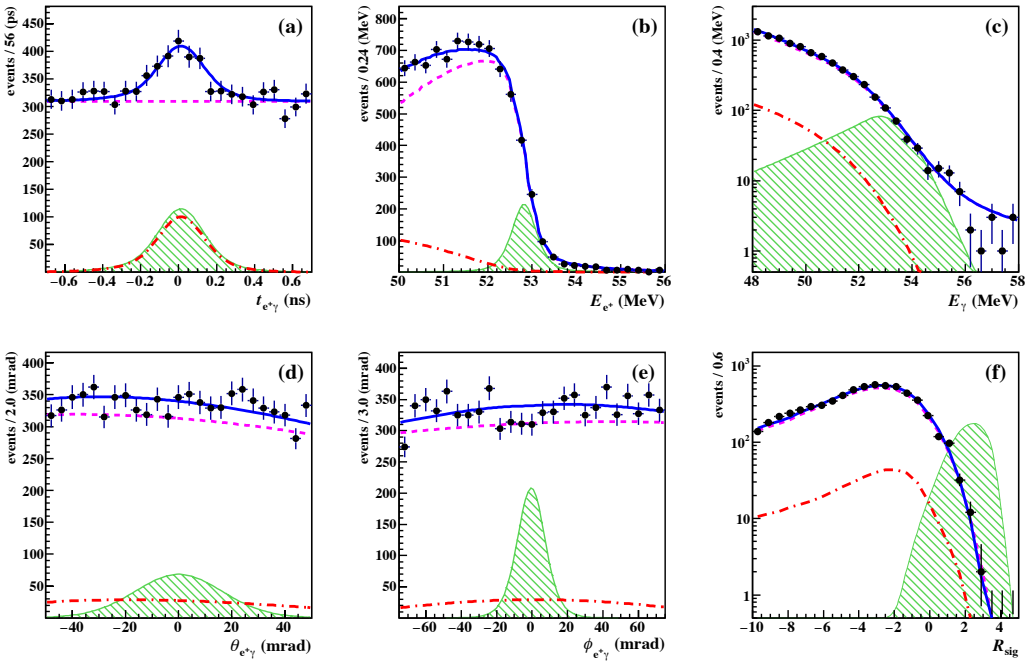

Figure 2: Data and PDFs from the analysis of the 2009-2013 data. Black dots: data. Blue: Total PDF. Magenta: accidental background. Red: RMD background. Green: Expected signal for a BR equal to 100 times the upper limit. See the text for the definition of $R_{\rm sig}$ the bottom-right plot.

reduce badly controlled light reflections, the improvements are expected to bring the photon energy resolution down to $\sim 1\%$. Moreover, the improved granularity of the readout in the inner face will strongly improve the photon position measurement and the capability to discriminate signals produced by two piled-up photons, allowing us to reduce the background.

The 16 DC modules will be replaced by a unique cylindrical drift chamber operated with a Helium:Isobutane (85:15) gas mixture and assembled with stereo wires in order to measure the coordinate along the beam axis. Prototypes [5] demonstrated the capability of reaching a resolution of about 110 μm in the radial coordinate, so that an energy resolution of about 120 keV and angular resolutions below 5 mrad are expected. The drift chamber will also cover a longer range along the beam axis ($\pm$ 1 m from the target). It will strongly reduce the untracked positron flight length, making negligible the track length contribution to the $T_{e\gamma}$ resolution. The TC-DC matching efficiency will be also doubled for the same reason. The wiring of the drift chamber just started, and the detector is expected to be delivered at the beginning of 2017.

The TC will be replaced by a new detector composed of hundreds of scintillator tiles read out by silicon photomultipliers (SiPM). The main advantage of this design is that each track will cross several tiles, so that the timing information from all of them can be combined to get a more precise positron timing. A resolution of about 35 ps is expected. The detector has been already partially installed and tested at PSI. The complete detector will be delivered by the end of 2016.

The largely increased number of readout channels required a new design of the trigger and DAQ architecture. In MEG-II trigger and DAQ will be collected in a single, compact system

(TDAQ). Each TDAQ crate will serve up to 256 channels in 16 boards, with digitization based on the DRS4 chip, basic trigger capabilities provided by each board and higher level trigger algorithms implemented in a trigger concentration board.

The improvement of the resolutions will allow us to increase the muon beam rate up to 7×10^8 muons per second. Starting on 2017 and after 4 years of data taking we expect to reach a sensitivity of about 6×10^{-14}, one order of magnitude below the MEG sensitivity.

References

[1] R. H. Bernstein and P. S. Cooper, Phys. Rept. **532** (2013) 27.

[2] J. Adam *et al.*, Eur. Phys. J. C **73** (2013) no.4, 2365.

[3] A. M. Baldini *et al.* [MEG Collaboration], arXiv:1605.05081 [hep-ex].

[4] A. M. Baldini *et al.*, arXiv:1301.7225 [physics.ins-det].

[5] A. M. Baldini *et al.*, JINST **11** (2016) no. 07, P07011.